CLK-peptides as superior surface stabilizers for silver nano structures: Role of peptide chain length

Manuel Ahumada,[a‡] Erik Jacques,[a‡] Cristina Andronic,[a] Jeffrey Comer,[c] Horacio Poblete,[d*] Emilio I. Alarcon[a,b*]

[a]Bio-Nanomaterials Chemistry and Engineering Laboratory, Division of Cardiac Surgery, University of Ottawa Heart Institute, 40 Ruskin Street, Ottawa, Ontario, K1Y 4W7, Canada. [b]Department of Biochemistry, Microbiology, and Immunology, University of Ottawa. [c]Institute of Computational Comparative Medicine, Nanotechnology Innovation Center of Kansas State, and Deparment of Anatomy and Physiology, Kansas State University, Kansas, USA. [d]Center for Bioinformatics and Molecular Simulations, Facultad de Ingeniería, Universidad de Talca, Chile. †Authors contributed equally to this work.

Supporting Information Placeholder

ABSTRACT: Three new collagen mimetic peptides containing the CLK motif as anchoring arms were tested for silver nanoparticle surface stabilization. Our experimental and molecular dynamic data indicate that peptide length does have an important effect in the resulting nanosilver's colloidal stability and biological performance.

Nanomaterials have become the building blocks for the next generation of materials in a variety of fields including biomedicine. This has ramped the pursuit of new strategies in nanoparticle surface stabilization.[1] Nanosilver has been one of the most studied nanomaterials for biomedical applications due to its unique electrical, optical, and chemical properties.[2] Thus, a large number of protecting agents and surface modifications have been attempted for improving its *in vivo* stability.[3-5] Protecting agents like citrate and thiols can provide cost-effective surface stabilization; however, such protection has proven to be suboptimal under physiological conditions.[6] Other approaches include the use of polymers, poly-peptides, proteins, or glycosides; but those are still far from being realistically scalable for commercial nanoparticle production, and additionally the binding motifs involved in the surface stabilization remain unknown. Furthermore, in the field of tissue engineering and regenerative medicine, there is an urgent need to combine nanosilver's biological function with structural components that allow safe incorporation of the material within biomimetic templates. Some attempts have used proteins and other polypeptides to anchor the nanostructures to the biomatrix. However, a general understanding of the effects of chain charge, binding mode and cooperativity remain unanswered. Recently, our team reported a new amino acid sequence CLKRS which at micromolar concentrations is capable of stabilizing spherical nanosilver.[7] However, the resulting nanocomposites lack long-term stability in solution. In the present work, we have used a combination of experiment and molecular dynamics for unveiling the molecular mechanisms involved in the interaction between nanometric silver and three novel collagen-like peptides; CLK-(GP-Hyp)$_n$ with n = 1, 3, and 5 (see Scheme 1). We further assessed the suitability of these novel composite materials for being incorporated within 3D collagen matrices.

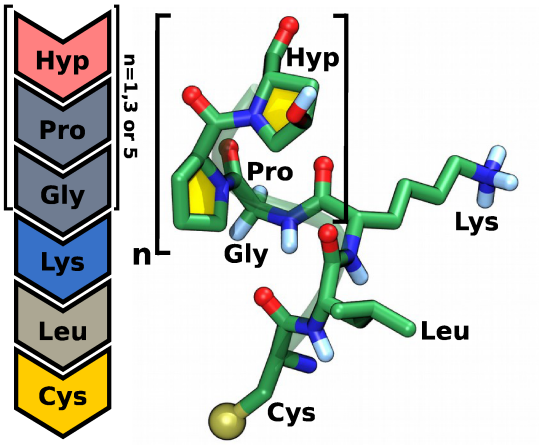

Scheme 1. Structural and sequence representations for the peptide sequences tested for nanosilver surface stabilization. Numbers shown in the left correspond to the repetitions of GP-Hyp in the different sequences.

Fig. 1 left shows the changes in absorption maxima, intensity and full width at the half maximum (FWHM) of each peptide in relation to its concentration, observables that are directly related to the nanocomposite's aggregation state. From these plots, it can be clearly seen that all the peptides, CLK-GP-Hyp (P1), CLK-GP-$(Hyp-GP)_2$-Hyp (P2), and CLK-GP$(Hyp-GP)_4$-Hyp (P3) show distinctive features when compared to the CLKRS sequence. Thus, for P1–P3, there was a red shift in the position of the absorption maximum (≈8 nm at 20 μM and ≈11 nm at 100 μM), alongside a ≈20% decrease in the SPB absorption intensity. Furthermore, FWHM values also increased by ≈ 7.0 and ≈ 11 nm at 20 and 100 μM peptide concentrations, respectively. These changes were considerably smaller than those for CLKRS, which had reductions of 50 and 70% absorption intensity at 20 and 100 μM, accompanied of 30 and 80 nm maxima position shifts and 68 and 180 nm FWHM, respectively. Note that precipitation of the nanosilver composite was not observed for the samples containing P2 and P3; however, P1 had reduced stability at >20 μM, *vide infra*. Fig. 1 right depicts a representative set of absorption spectra of citrate-capped nanosilver (AgNPs@citrate) measured in the presence of 20 μM concentrations for peptides P1–P3 and/or CLKRS, which clearly illustrates differences between CLKRS and P1–P3.

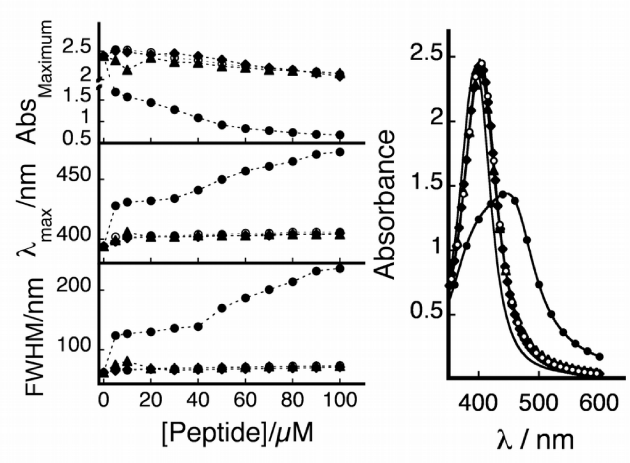

Figure 1. Effect of peptide addition on the surface plasmon band (SPB) for CLKRS (▽), CLK-GP-Hyp (▽), CLK-GP-$(Hyp-GP)_2$-Hyp (▽), and CLK-GP$(Hyp-GP)_4$-Hyp (▽). Left (Top): Changes in SPB maximum intensity as a function of the peptide concentration. (Middle): Variation of SPB maximum position measured at the different peptide concentrations. (Bottom) Full width at half maximum (FWHM) values calculated from SPB fitting to a single Gaussian curve (Kaleida Graph®) at different peptide concentrations. Right: Representative SPB spectra for spherical nanosilver measured at 20 μM peptide concentrations. The nanosilver control sample without peptide is also included (black line with no symbols). All measurements were carried out at room temperature using 1 cm pathlength cuvettes (n=3).

Nanoparticle hydrodynamic diameter increased 10 times upon adding P1 > 20 μM, which further increased to up to 42 times at 100 μM (Fig. 2a). Colloidal silver solutions containing P1 > 20 μM did not remain stable and precipitated after 2 h (not shown). No statistically significant differences, when compared to the control without peptide, in sizes were observed for P2 and P3 (7.0±1.0 nm, $p>0.1$). When monitoring changes in the nanoparticle surface charge (see Fig. 2b) as a function of the peptide concentration, 100 μM of P1 did not produce complete surface charge neutralization. However, for P2 and P3 peptide concentrations >20 μM switched the charge of the composite material from −30 to +3.0 mV. Increasing the concentration of P1 led to a net decrease in the SPB and band broadening, which can be interpreted as a direct consequence of supramolecular assembly of P1 around the

nanoparticle. No significant differences are observed for nanoparticles protected with P2 and P3 at either concentrations. Furthermore, the effect of ionic strength using 0.9% NaCl as a biological mimetic medium for up to 48h, showed improved surface stability that follows P3 > P2 >> P1, see Fig. 2c. In addition, the effect of the pH was assessed between 6.3-9.5 values for nanosilver containing P2 and P3 at 20 and 100 µM showing little effect of pH variation, see Fig. S1.

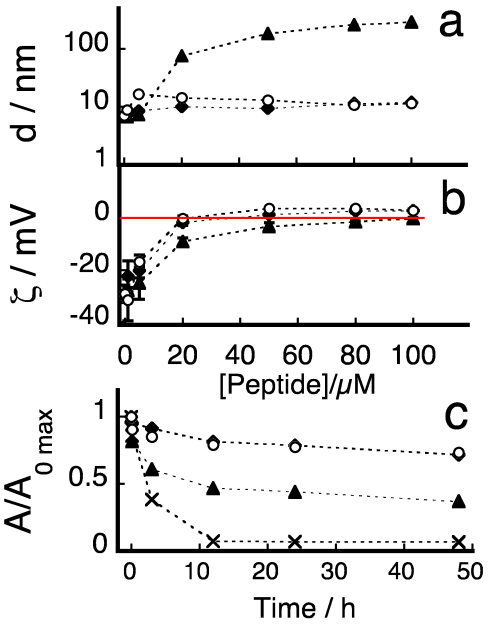

Figure 2. Effect of peptide addition on the nanoparticle hydrodynamic size **(a)** and surface charge **(b)** for CLK-GP-Hyp (⊣), CLK-GP-(Hyp-GP)$_2$-Hyp (▲), and CLK-GP(Hyp-GP)$_4$-Hyp (◡). **(c)** Changes in surface plasmon band maximum absorption measured for citrate protected nanosilver in the presence of 20 µM of the peptides CLK-GP-Hyp (⊣), CLK-GP-(Hyp-GP)$_2$-Hyp (▲), and CLK-GP(Hyp-GP)$_4$-Hyp (◡) at different time points when incubated in 0.9% NaCl solution. The nanosilver control sample without peptide is also included (X). All measurements were carried out at room temperature by triplicate, see SI for further details.

Moreover, one of the limitations that still remains for most capping agents is their stability for in a useful range of temperatures. Fig. 3 shows the effect of heating silver nanoparticle samples containing 20 µM of P2 and P3 as well as a comparative sample prepared using 20 µM human serum albumin (HSA) at ≈100°C. In contrast to the solution containing the HSA protein, the samples prepared with the peptides remained stable in solution, with just a minor change in the SPB (<10%) within the first 45 min after heating. Those are remarkable differences, which as a whole demonstrate the superiority of P2 and P3 over common protein surface capping of nanosilver. Heating of the HAS capped samples led to almost instantaneous and irreversible changes of the nanosilver SPB.[8] Similar results were previously reported by our group for citrate capping agent replacement with type I collagen.[9]

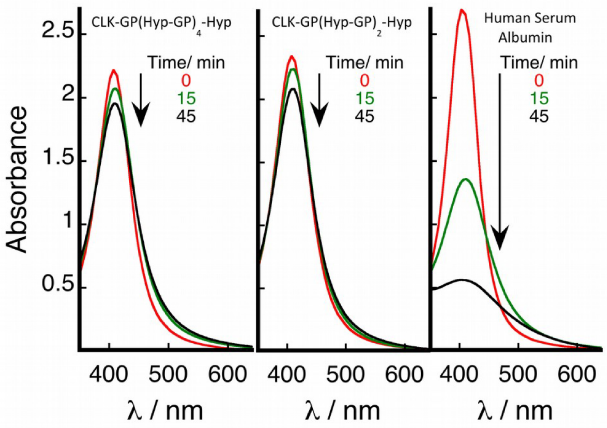

Figure 3. Changes in nanosilver SPB seen after sample solution heating for up to 45 min at 98ºC. Nanosilver samples were prepared using 20 µM of the CLK-GP-(Hyp-GP)$_4$-Hyp, CLK-GP(Hyp-GP)$_2$-Hyp or human serum albumin (HSA). Samples were measured at different time points after heating. All measurements were carried out at room temperature, see SI for further details.

Molecular dynamics simulation coupled with free-energy calculation techniques enabled us to determine the likely binding modes of the peptides P1, P2 and P3 on the nanosilver surface. Using the adaptive biasing force[10-13] technique, we determined the free energy landscape for peptide adsorption, considering both the distance between the surface and peptide (Z), as well as the peptide's orientation relative to the surface (ζ). Taking the z axis to be perpendicular to the silver{111} surface, Z was defined as the difference in the z coordinates of the center of mass of the peptide and plane passing through the centers of the first layer

of silver atoms. The second transition coordinate, ζ, was defined by the difference in the *z* coordinates (the *z* axis being perpendicular to the surface) of the center of mass of the last and first residues of the peptide. Fig. 4 left shows the two-dimensional free energy landscape (potential of mean force) as a function of *Z* and ζ calculated for each peptide. The high-affinity areas (blue) represent conformations in which the peptide interacts most strongly with the surface, while the yellow, green and cyan regions indicate lower affinities. Areas shown in red are high free-energy conformations, corresponding to steric clashes between the surface and peptide (small *Z* values) or unfavorable extension of the peptide (large ζ values).

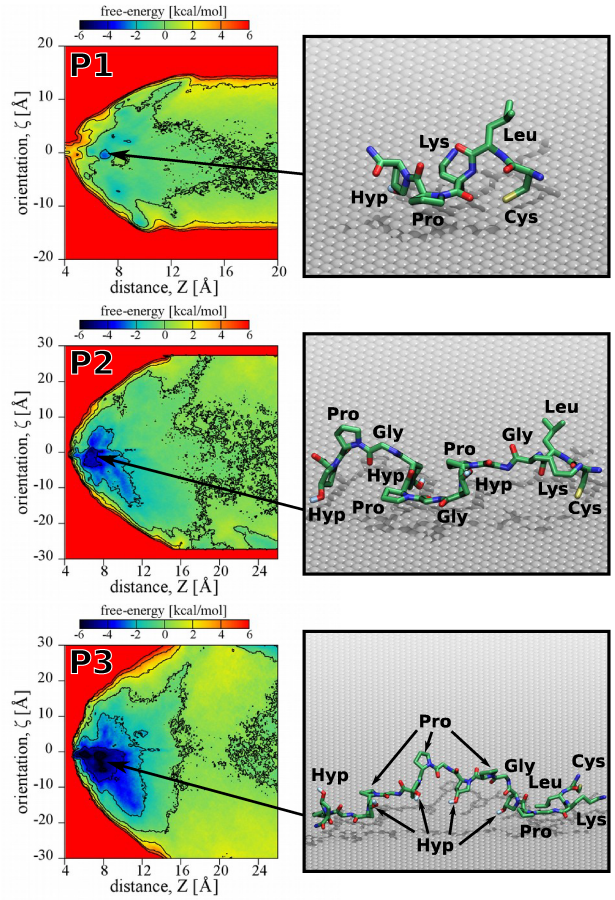

Figure 4. Molecular simulations of the adsorption of P1, P2 and P3 to the nanosilver surface. (Left) Two-dimensional free energy landscape for the peptides P1, P2 and P3. By convention, the free energy is anchored to average to zero for large separations of the peptide and surface (*Z*>24 Å). The black curves represent isoenergetic contours separated by 2 kcal/mol. (Right) Typical conformations of each peptide corresponding to the free energy minima in the two-dimensional free-energy plots indicated by the black arrow.

The lowest free energies occur when the peptide centers of mass are about 6.5 Å from the surface and the peptides lie roughly flat against the surface (ζ ≈ 0). The peptide affinity for the surface is ranked P3 > P2 >> P1, in agreement with our experimental data, corresponding to free energies of −5.0, −3.4 and −1.5 kcal/mol, respectively (see Fig. S3). Fig. 4 right shows representative conformations near the global free energy minimum for each peptide. Interestingly, in all three cases, contact between the surface and the N-terminal thiol group is favored, even when the center of mass of the peptide is relatively far from the surface.

Additionally, the OH^- group of the Hyp amino acids tended to be directed toward the silver surface, helping the peptides to attain planar conformations, which increases the peptide-surface contact area and stabilizes their adsorption. Overall, the free energy results show that increasing the peptide length by the number of Hyp groups enhances affinity for the surface, which is clearly observed in the two-dimensional free energy landscape for each peptide.

The ability of the peptides to act as protecting agents for unprotected nanoparticles, was also evaluated by using micromolar concentrations of the peptides, see Fig. S4. Fig. 5a shows representative absorption spectra for silver nanoparticles synthesized in the presence of 1.0 μM of P3. Notably nanoparticle SPB intensity reaches a plateau (≈2.0±0.2, *n*=4) within 5 minutes of nanoparticle synthesis. Similar results were observed for P2, see Fig. S4 inset, while P1 produced stable nanoparticles only at concentrations ≥ 5.0 μM. Fig. 5b summarizes silver nanoparticle size distributions measured by transmission electron microscopy (TEM). Interestingly, the nanoparticles prepared using P3 had considerably smaller diameter than those prepared with other compounds (Fig. 5b), including those prepared in this work (15 vs. 35 nm, for P3 and P2, respectively) and those previously reported when proteins were used as protecting agents for nanosilver.[14] Nanoparticle sizes for P2 and P3

showed no dependence with the peptide concentration, which suggests that surface protection occurs more effectively for P3 than for P2.

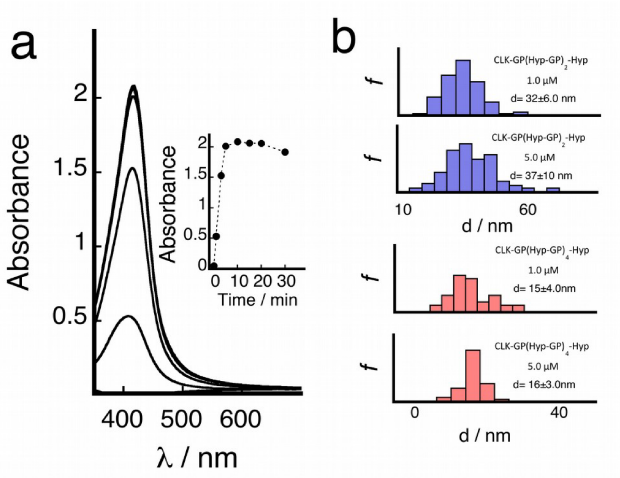

Figure 5. **(a)** SPB for nanosilver measured at different time points from bottom to top, 0, 1, 3, and 5 minutes upon UVA irradiation of the solution containing the nanosilver precursors in the presence of 1.0 μM of CLK-GP(Hyp-GP)$_4$-Hyp. Inset: Representative changes in the SPB maxima absorption measured at different time intervals during the synthesis. All measurements were carried out at room temperature, see SI for further details. **(b)** Size histograms for silver nanoparticles prepared using two different concentrations of the peptides CLK-GP(Hyp-GP)$_2$-Hyp and CLK-GP(Hyp-GP)$_4$-Hyp as protecting agents for photochemically formed nanosilver. Histograms were constructed by measuring 100 individuals nanoparticles from TEM images. Mean number and standard deviations for each population are shown in the figures.

Considering that P3 has the highest affinity for the nanosilver surface, we performed a comprehensive analysis of its free energy pathway, starting from the aqueous environment to reach the adsorbed conformation to nanosilver. Fig. 6 (Left) shows a surface plot of the free-energy landscape as a function of the two transition coordinates *Z* and ζ previously discussed. The red arrow represents the most probable pathway in the adsorption process. As shown in Fig. 6 right, three typical peptide conformations were identified at distances of 6.5 Å, 10.5 Å and 23 Å, labeled as A, B and C, respectively. Conformation C shows a random positioning of the cysteine thiol group with respect to the last residue of the peptide, which is a typical conformation of the free peptide in bulk solution. The lowest free energy path to the adsorbed state involves contact between the N-terminal cysteine amino acid (Fig. 6B), which favors the subsequent adsorption of the entire peptide. Similar results for CLK peptides were previously reported by our group.[7] Finally, conformation A shows the most favorable structure of the P3 peptide at the position global free energy minimum in *Z* and ζ. Here, both the Cys and Hyp amino acids are in direct contact with the silver surface.

Finally, nanosilver protected by the synthesized peptides (either with P2 or P3) was chemically incorporated within type I collagen hydrogels, and the ability of these hydrogels to sustain cell proliferation and antimicrobial activities were assessed. Overall, P3 outperformed P2 in terms of producing hybrid materials that, for example, while allowing cell proliferation of human skin fibroblasts (Fig. S5), also prevented bacterial infection mediated by Pseudomonas aeruginosa, see Fig. S6.

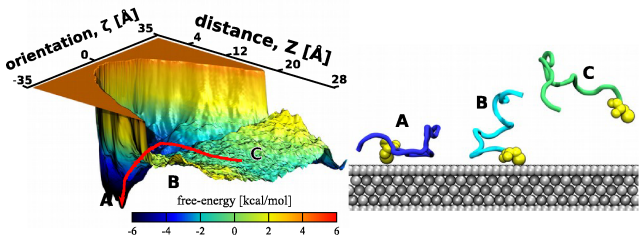

Figure 6. Most probable binding mode for P3. (Left) Surface plot of the free-energy landscape for P3 adsorption to the Ag{111} surface. A, B and C are typical conformations for P3 along the adsorption pathway (red arrow) from bulk solution to the nanosilver–water interface. Cysteine is represented by yellow spheres while the rest of the protein is shown as a tube with the color indicative of the associated free energy.

The conclusions section should come in this section

Designing of specific capping agents as peptides for nanosilver, using CLK motif as anchoring arms have shown to be highly

efficient to control of size and growth of nanosilver surfaces. Through both experimental and computational result indicate that the peptide length have a critical effect in the nanosilver is colloidal stability and biological performance.

ASSOCIATED CONTENT

Supporting Information. The Supporting Information is available free of charge on the ACS Publications website.

Materials and methods and SI figures (PDF)

AUTHOR INFORMATION

Corresponding Author

*ealarcon@ottawaheart.ca
*hopoblete@utalca.cl

ORCID

Emilio I. Alarcon: 0000-0001-5100-6179
Manuel Ahumada: 0000-0002-0589-3296
Horacio Poblete: 0000-0003-2650-3565
Jeffrey Comer: 0000-0003-4437-1260

Author Contributions

‡These authors contributed equally.

Funding Sources

No competing financial interests have been declared.

Any funds used to support the research of the manuscript should be placed here (per journal style).

Notes

(Word Style “Section_Content”). Any additional relevant notes should be placed here.

ACKNOWLEDGMENT

This work was made possible by funding from the Natural Sciences and Engineering Research Council (NSERC) to EIA RGPIN-2015-0632 and to the Canadian Institutes of Health Sciences (CIHR). EIA also thanks UOHI start-up grant 1255. EJ and CA acknowledge the undergraduate Student Research Awards Program from University of Ottawa and NSERC. HP thanks the academic program “Núcleo Científico Multidisciplinario” from Universidad de Talca-Chile and Fondecyt grant Nº 1171155. This work was supported in part by a grant from the National Science Foundation (CHE-1726332).

REFERENCES

1. A. Ravindran, P. Chandran and S. S. Khan, *Colloids and Surfaces B: Biointerfaces*, 2013, **105**, 342-352.
2. H. de Alwis Weerasekera, M. Griffith and E. I. Alarcon, in *Silver Nanoparticle Applications: In the Fabrication and Design of Medical and Biosensing Devices*, eds. E. I. Alarcon, M. Griffith and K. I. Udekwu, Springer International Publishing, Cham, 2015, DOI: 10.1007/978-3-319-11262-6_5, pp. 93-125.
3. M. P. Monopoli, D. Walczyk, A. Campbell, G. Elia, I. Lynch, F. Baldelli Bombelli and K. A. Dawson, *Journal of the American Chemical Society*, 2011, **133**, 2525-2534.
4. B. A. Aguilar-Castillo, J. L. Santos, H. Luo, Y. E. Aguirre-Chagala, T. Palacios-Hernandez and M. Herrera-Alonso, *Soft Matter*, 2015, **11**, 7296-7307.
5. T. L. Moore, L. Rodriguez-Lorenzo, V. Hirsch, S. Balog, D. Urban, C. Jud, B. Rothen-Rutishauser, M. Lattuada and A. Petri-Fink, *Chemical Society Reviews*, 2015, **44**, 6287-6305.
6. E. I. Alarcon, K. Udekwu, M. Skog, N. L. Pacioni, K. G. Stamplecoskie, M. Gonzalez-Bejar, N. Polisetti, A. Wickham, A. Richter-Dahlfors, M. Griffith and J. C. Scaiano, *Biomaterials*, 2012, **33**, 4947-4956.
7. H. Poblete, A. Agarwal, S. S. Thomas, C. Bohne, R. Ravichandran, J. Phospase, J. Comer and E. I. Alarcon, *Langmuir*, 2016, **32**, 265-273.
8. E. I. Alarcon, C. J. Bueno-Alejo, C. W. Noel, K. G. Stamplecoskie, N. L. Pacioni, H. Poblete and J. C. Scaiano, *Journal of Nanoparticle Research*, 2013, **15**, 1374.
9. M. Ahumada, S. McLaughlin, N. L. Pacioni and E. I. Alarcon, *Analytical and bioanalytical chemistry*, 2016, **408**, 1993-1996.
10. J. Comer, J. C. Gumbart, J. Henin, T. Lelievre, A. Pohorille and C. Chipot, *Journal of Physical Chemistry B*, 2015, **119**, 1129-1151.
11. J. Comer, J. C. Phillips, K. Schulten and C. Chipot, *J Chem Theory Comput*, 2014, **10**, 5276-5285.
12. E. Darve and A. Pohorille, *J Chem Phys*, 2001, **115**, 9169-9183.
13. J. Henin and C. Chipot, *J Chem Phys*, 2004, **121**, 2904-2914.
14. M. Ahumada, E. Lissi, A. M. Montagut, F. Valenzuela-Henriquez, N. L. Pacioni and E. I. Alarcon, *Analyst*, 2017, **142**, 2067-2089.

SYNOPSIS TOC (Word Style “SN_Synopsis_TOC”). If you are submitting your paper to a journal that requires a synopsis graphic and/or synopsis paragraph, see the Instructions for Authors on the journal’s homepage for a description of what needs to be provided and for the size requirements of the artwork.

To format double-column figures, schemes, charts, and tables, use the following instructions:

Place the insertion point where you want to change the number of columns
From the **Insert** menu, choose **Break**
Under **Sections**, choose **Continuous**
Make sure the insertion point is in the new section. From the **Format** menu, choose **Columns**
In the **Number of Columns** box, type **1**
Choose the **OK** button

Now your page is set up so that figures, schemes, charts, and tables can span two columns. These must appear at the top of the page. Be sure to add another section break after the table and change it back to two columns with a spacing of 0.33 in.

Table 1. Example of a Double-Column Table

Column 1	Column 2	Column 3	Column 4	Column 5	Column 6	Column 7	Column 8

Authors are required to submit a graphic entry for the Table of Contents (TOC) that, in conjunction with the manuscript title, should give the reader a representative idea of one of the following: A key structure, reaction, equation, concept, or theorem, etc., that is discussed in the manuscript. Consult the journal's Instructions for Authors for TOC graphic specifications.